JCRS

Journal of Chemical Reactivity and Synthesis 2025: 15(2) 107-127

Research Article

Investigation of Adsorption Process and Kinetics of Sunset Yellow Dye Removal from Aqueous Solutions Using Zinc Metal-Organic Nano framework

Zahra Shariati [a,b], Mohammad Kazem Mohammadi[a*], Payam Hayati [c], Fazlolah Eshghi[d]

[a] Department of Chemistry, Ahv.C., Islamic Azad University, Ahvaz, Iran

[b] Department of Chemistry, SR.C., Islamic Azad University, Ahvaz, Iran.

[c] Department of Biotechnology and Life Sciences, University of Insubria, Via Jean Henry Dunant, 3, 21100 Varese, Italy

[d] Department of Chemistry, College of Sciences, Shiraz University, Shiraz, Iran

ABSTRACT

The surface adsorption and removal of several azo and non-azo dye compounds used in the food and dye industries, which enter environmental wastewater after use, were investigated using nano-adsorbents. The anionic Sunset Yellow dye used in this research is a sulfone azo food dye that is water-soluble and employed for coloring various products in the food industry, such as sugar cane production, dietary supplements, soft drinks, jelly, fruit juices, and more. The results showed that the highest removal percentage of Sunset Yellow dye using zinc metal-organic framework occurs at pH 5, with efficiency decreasing at higher or lower pH values. The highest removal percentage of Sunset Yellow dye was achieved with 0.5 g/L of zinc oxide nano-adsorbent. The results indicated that the highest removal percentage for Sunset Yellow dye occurred within 40 minutes using the nano-adsorbent

Keywords: Surface adsorption – Metal-organic framework – Sunset Yellow – Zinc nano-metal

ARTICLE INFO

Received: 29 December 2025
Accepted: 17 January 2026
Available: 18 January 2026

✉: M.K. Mohammadi
mkmohamadi@iau.ac.ir

10.82437/jcrs.2025.1229987

Introduction

Water resource pollution due to industrial wastewater discharge has become one of the global environmental crises [1]. Among various pollutants, synthetic dyes used in industries such as textiles, leather, paper, and cosmetics have a significant share. Over 700,000 tons of dyes are produced annually worldwide, with 10-15% discharged as wastewater. These compounds, mainly featuring complex multi-ring aromatic structures (such as azo,

anthraquinone, and triphenylmethane)[2] , are highly resistant to biological, photolytic, and chemical degradation. Even low concentrations (less than 1 ppm) of these dyes in water not only create an undesirable appearance but also reduce sunlight penetration, disrupting photosynthesis and threatening aquatic ecosystems [3]. From a human health perspective, many of these dyes and their metabolites (such as benzidine and aromatic amines) are known to be toxic, mutagenic, and carcinogenic (Chung, 2016). Therefore, efficient removal of these pollutants before entering the environmental cycle is an undeniable necessity.

Numerous methods are employed for treating colored wastewater, including physical processes (such as adsorption, membrane filtration), chemical processes (coagulation-flocculation, advanced oxidation), and biological processes [4]. Among these, surface adsorption is considered one of the most efficient and widely used techniques due to its simple design, high efficiency, relatively low cost, and adsorbent recyclability [5]. The performance of this method strongly depends on adsorbent properties such as specific surface area, porosity, surface functional groups, and chemical stability. Common adsorbents like granular activated carbon, clay, zeolite, and agricultural wastes, while applicable, often suffer from limited adsorption capacity, slow kinetics, and low selectivity [6].

In the past two decades, the emergence of nanotechnology and nano-adsorbent design has opened new horizons in water treatment. Nano-adsorbents, due to their high surface-to-volume ratio, abundant active surface sites, tunable porosity, and targeted chemical modification capabilities, significantly enhance adsorption capacity and kinetics [7]. These nanomaterials can form stronger interactions (such as van der Waals forces, hydrogen bonding, electrostatic interactions, and complexation) with dye molecules. Prominent nano-adsorbents include metal oxide nanoparticles (e.g., Fe_3O_4, ZnO, TiO_2), carbon nanotubes, graphene and graphene oxide, polymeric nanocomposites, and especially metal-organic frameworks (MOFs**)** [8-9]. These nanostructures not only act as direct adsorbents but can also

serve as supports for catalysts in advanced oxidative degradation processes, enabling combined removal (adsorption with degradation) [10]. However, challenges such as nanomaterial leakage into the environment, synthesis costs, and efficient post-treatment separation remain subjects of ongoing research [11]. Nevertheless, the high potential of nano-adsorbents in providing effective, selective, and sustainable solutions for colored pollution has made them a focal point in environmental engineering research [12-20].

Increasing industrial activities have led to massive production of wastewater containing persistent organic pollutants. Among these, synthetic pigments widely used in textile, leather, paper, and printing industries hold a special place. These compounds, often with complex aromatic structures, are not only toxic and potentially carcinogenic but also highly resistant to biological and photodegradation, posing serious threats to aquatic ecosystems and human health[21] . Conventional water treatment methods like coagulation, activated carbon adsorption, or biological processes are often ineffective in completely removing these dyes, as they merely transfer phases without full degradation. Thus, developing advanced technologies with high efficiency, suitable selectivity, and cost-effectiveness is a scientific and industrial necessity.

In this context, metal-organic framework (MOF) nanomaterials, as an advanced class of crystalline porous materials, have revolutionized materials science and chemical engineering over the past two decades. MOFs consist of inorganic building units (metal ions or clusters) linked by bi- or multi-dentate organic ligands. This unique architecture provides materials with exceptional properties, including ultra-high specific surface area (over 7000 m^2/g), uniform and tunable nanoscale porosity, and extensive design and functionalization capabilities [22]. These features make MOFs ideal candidates for advanced applications in gas storage, catalysis, drug delivery, and especially water treatment.

The application of MOFs in the removal of colored pollutants is mainly based on two main mechanisms: surface adsorption and photocatalytic degradation. Thanks to their very high specific surface area and tunable porosity, MOFs can trap very large amounts of dye molecules in their cavities. The interactions involved in this process include van der Waals forces, hydrogen bonding, π-π interactions between the aromatic rings of the ligand and the dye, and electrostatic interactions between the MOF surface and the charge of the dye molecule[23]. For example, the well-known zirconium-based MOF UiO-66 has shown remarkable performance in the adsorption of cationic dyes such as methylene blue due to its excellent chemical and aqueous stability as well as the presence of Lewis acid sites [24].

In addition to adsorption, some MOFs with semiconducting structures (such as the MIL-53(Fe), MIL-100(Fe) and ZIF-8 series) can act as efficient photocatalysts under visible or ultraviolet light irradiation. In this process, photons of light excite electrons and create charge carriers (electrons and holes) in the MOF structure. These charge carriers can react with oxygen or water to produce powerful reactive oxygen species (ROS) such as hydroxyl radicals (•OH) and superoxide ($•O_2^-$). These reactive species non-selectively oxidize complex organic dye molecules and eventually decompose into harmless products such as water, carbon dioxide and inorganic salts[25]. This mechanism, unlike adsorption, destroys the pollutant and overcomes the problem of saturation and recycling of the adsorbent.

The key advantage of MOFs in this area is their rational design capability. By intelligently selecting the metal node (Fe moieties for photocatalytic activity or Zr for stability) and designing the organic ligand (in terms of length, porosity created, and functional groups), researchers can synthesize a structure that is specifically optimized to target a specific color pollutant or a range of pollutants. Also, the possibility of post-synthesis modification or creation of composite structures with materials such as graphene oxide or nanoparticles

provides a wide window for improving performance, stability, and recyclability over multiple cycles.[26] .

Consequently, metal–organic nanosheets, with their unique combination of excellent surface area, tunable porosity, stability, and catalytic activity, are a promising answer to the challenge of removing persistent color pollutants from the environment. Future research will likely focus on scaling up synthesis, improving water stability under real-world conditions, and designing smart structures with easy recyclability and reuse.

2. Experimental

2.1. Materials

All chemicals used in this research were of high purity, and all solutions were prepared with double-distilled water. Table 1 lists the chemicals used, while Table 2 and Figure 1 provide the chemical-physical properties and structure of the studied dyes

Table 1 . Materials Used

	Material Name	Manufacturer	Country
1	Zinc oxide nano-adsorbent	Solarbio	China
2	Sunset Yellow dye powder	Sigma	USA
3	Double-distilled water	-	Iran

Table 2. Physical and Chemical Properties of Studied Dyes

Dye	Molecular Formula	Molecular Weight (g/mol)	Melting Point (°C)	λ_max (nm)
Sunset Yellow	$C_{16}H_{10}N_2Na_2O_7S_2$	452.37	300	458

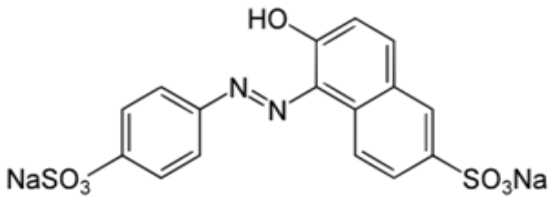

Fig. 1. Structure of Sunset Yellow dye

2.2. Instruments

pH meter, jar test apparatus, centrifuge, single-wavelength UV spectrophotometer

2.2.1. Instrument Calibration

The desired wavelength is set, and a cell containing blank or solvent (double-distilled water) is placed in the light path. The light control knob is adjusted so A=0. Standard solutions of initial concentrations are then prepared, and absorbance (A) at the maximum wavelength is measured for each. A calibration curve of absorbance vs. concentration is plotted

2.3.Synthesis of Zinc(II)-Imidazole Metal-Organic Supramolecular Nanostructure

Hydrothermal Method

0.798 g (2.5 mmol) zinc iodide (ZnI_2) was dissolved with 5 mmol imidazole (Im) in 20 mL double-distilled water. The mixture was stirred continuously at room temperature (25±2°C) for 30 minutes to ensure complete dissolution. The homogeneous solution was transferred to a pressure-resistant autoclave and placed in a programmed oven. The temperature was gradually raised to 120°C for 48 hours. The system was then slowly cooled to room temperature to allow crystal growth. After 10 days at ambient conditions, formed crystals were separated and washed with pure acetone. Some crystals were sent for single-crystal X-ray diffraction (SCXRD), while the rest were dried and analyzed by FT-IR, powder X-ray diffraction (PXRD), and scanning electron microscopy (SEM). The overall reaction is

: $\mathbf{ZnI_2 + Im + water \rightarrow \{ZnX_2(Im)_2\}}$.

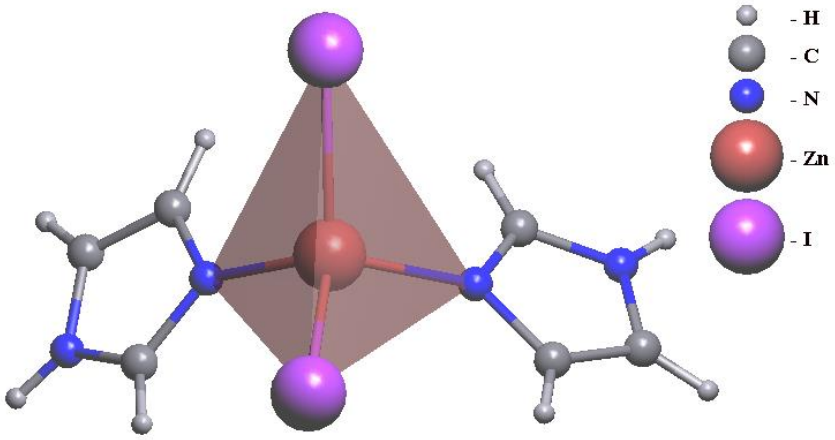

Fig. 2. The coordination environment around zinc atoms in complex 1, as ascertained through single-crystal X-ray diffraction, demonstrates a distorted tetrahedral N_2I_2 geometry that is a consequence of the coordination with two imidazole ligands and two iodide ions.

3. Results and Discussion

3.1.Methods for identifying the supramolecular nanostructure of Zn-MOF

3.1.1 .Morphology of the supramolecular nanostructure of Zn-MOF

SEM image in Figure 2 shows layered structures in the microscale. This sample, synthesized without ultrasound at 50°C, exhibits regular morphology with distinct layered structure. Absence of ultrasound allows free crystal growth and larger structures.

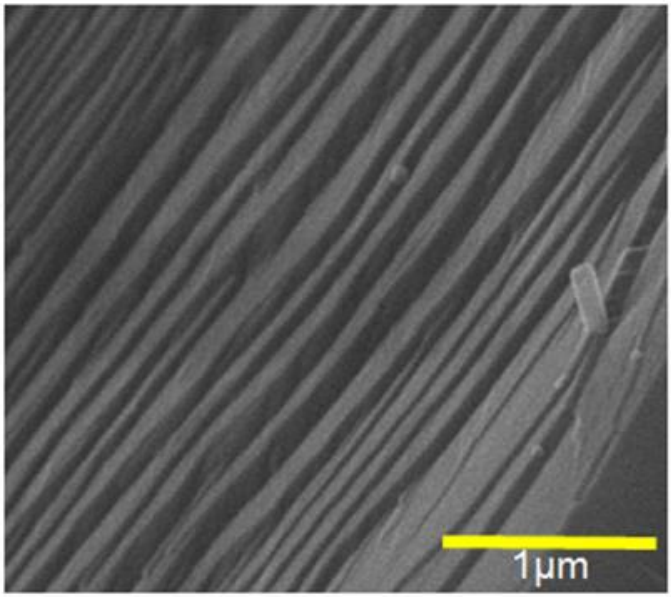

Fig. 3. Morphology of Zn-MOF nanostructure without sonication

With 60 W ultrasound at the same temperature, morphology shifts to smaller particles and mixed structures, indicating acoustic cavitation's impact on nucleation and growth (Figure 3)

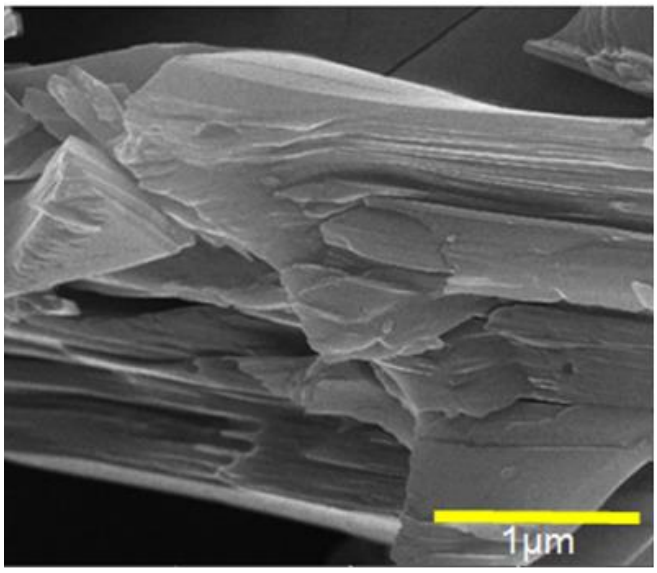

Fig. 4. Morphology of Zn-MOF nanostructure under 60 W sonication

At 60 W ultrasound and 70°C, nanoparticles with minimal aggregation form, optimal for nanoscale structures with good disperson (Figure 4)

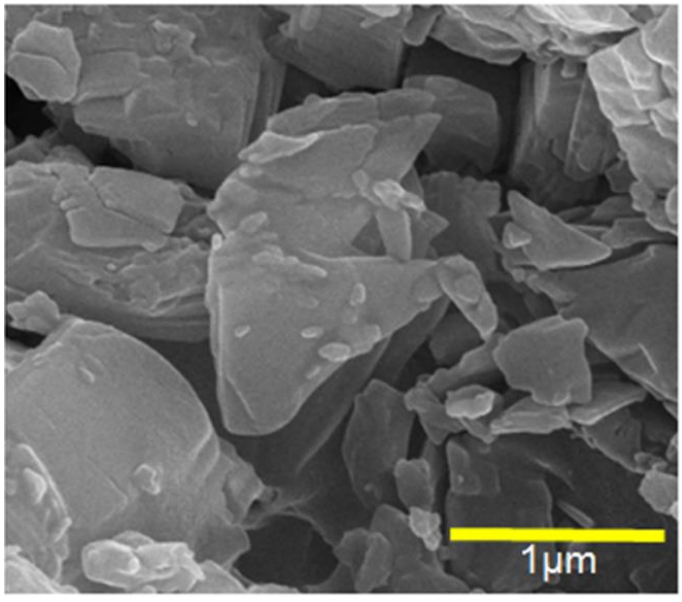

Fig. 5. Morphology of Zn-MOF nanostructure under 60 W sonication at 70°C

One of the most critical mechanisms in the sonochemical method for the synthesis of metal-organic frameworks (MOFs) is the role of acoustic cavitation. Through this phenomenon, ultrasound waves create bubbles in the reaction medium, whose violent collapse leads to the generation of shock waves and high-energy microcurrents. This controlled localized energy leads to several desirable outcomes: first, particle size control, which significantly reduces their average size from the micro to nanoscale. Second, improved material dispersion, which prevents particle aggregation and helps create a more uniform size distribution. Finally, the smaller particles produced will have a higher specific surface area, which is crucial for catalytic and storage applications.

In addition to cavitation, temperature also plays an important role in controlling the final product. It has been observed that increasing the temperature from 50 to 70 °C has significant effects on the synthesis process. Higher temperature facilitates mass transfer and improves

the solubility and diffusion of ions, which increases the availability of starting materials for the reaction. Also, increasing the temperature helps in thermodynamic control of the process and optimizes the balance between nucleation and crystal growth. From a kinetic perspective, higher temperature reduces the energy barrier and coordination reactions between the metal ion and the organic ligand occur more easily. Investigation of the mechanism of formation of layered structures in different samples shows that the synthesis conditions affect the orientation of crystal growth. The sonochemical method allows for control of crystal growth geometry through the precise adjustment of three main factors: growth direction control by determining the preferred directions for crystal growth, nucleation rate tuning by controlling the number of nucleation centers that form, and mass transfer management by improving material transport to the growing surface, ensuring product distribution and quality.

These findings are consistent with related studies in the field of nanomaterials and MOFs. For example, in the field of sonochemical synthesis of zinc oxide (ZnO), Morales-Flores et al. have shown that changing the pH and sonication conditions can change the morphology of ZnO nanostructures from rod-like to spherical, which is consistent with our observation regarding the effect of synthesis conditions on the morphology of MOFs. Also, Arruda et al. reported that a 17-h sonication treatment resulted in a 70% reduction in the size of ZnO crystals, which also confirms the effect of applying 60 W of sonication power on the significant reduction in particle size in the present study. Finally, various studies in the field of the effect of temperature on MOFs emphasize that the reaction temperature directly affects the topology and dimensions of the structures and that increasing the temperature usually leads to the formation of more complex three-dimensional structures, which is consistent with the results observed for samples synthesized at higher temperatures.

3.1.2 .FT-IR Spectroscopy Analysis of Zn-MOF Nanostructure

The region at 3048 cm-1 is related to the C-H stretching vibrations of aromatic rings. The presence of this peak indicates the presence of aromatic rings in the imidazole ligand structure. The position of this peak is almost the same in both samples, however, its intensity is higher in the sonicated sample. These results indicate the preservation of the aromatic structure of the ligand during the synthesis process.

Figure 5 shows that in both compounds, a strong peak is observed in this region at 1600 cm-1, which is related to the aromatic C=C stretching vibrations. This peak is a characteristic of the presence of aromatic rings in the MOF structure and confirms the formation of a coordination bond between the metal and the ligand. In the 1400 cm-1 region, the peak represents the C=N stretching vibrations of the imidazole ring, the presence of which is of particular importance because it indicates the success of the coordination process between the nitrogen atoms of the imidazole ligand and the zinc metal center.

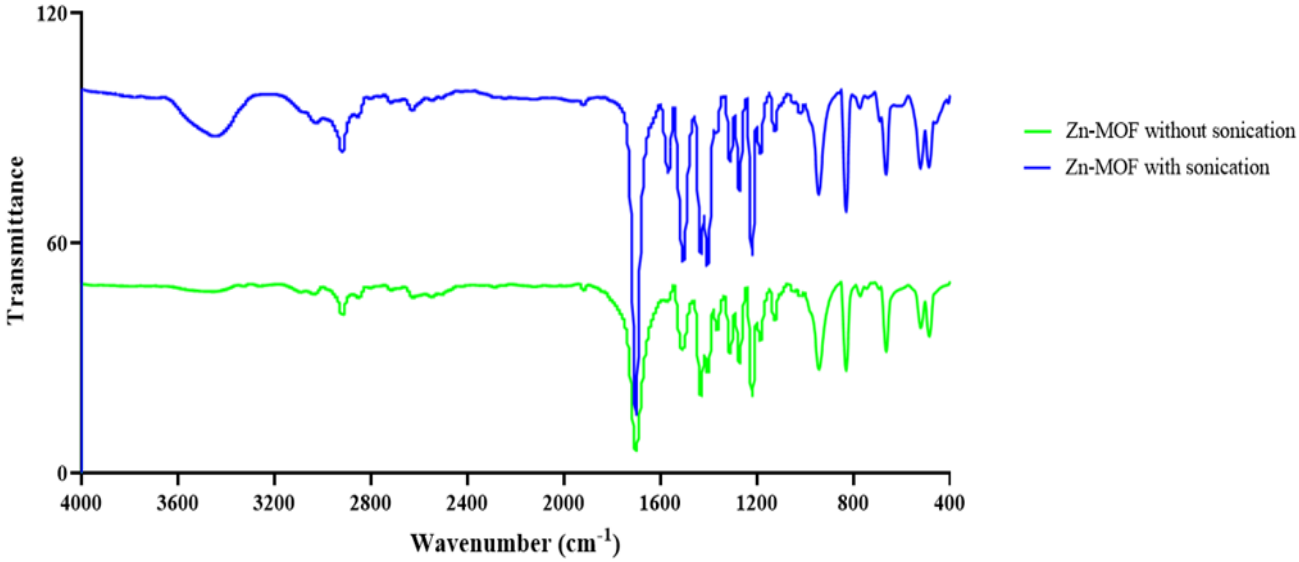

Fig. 6. FT-IR spectra of Zn-MOF frameworks with and without ultrasound

Based on the results of Fourier transform infrared (FT-IR) spectroscopy analysis, the successful formation of the zinc-imidazole metal-organic framework (MOF) nanostructure is fully confirmed. This is confirmed by the simultaneous presence of key peaks related to the imidazole ligand (observed at around 3048 cm-1, 1600 cm-1 and 1400 cm-1) as well as metal-ligand vibration peaks in the low frequency region (around 1500 cm-1). Furthermore, one of the most important evidences of MOF formation and complete coordination is the absence of free N-H stretching peaks, which are usually observed in the range of 2500 to 3000 cm-1; the absence of these peaks indicates that the N-H groups of imidazole are fully involved in the coordination bond with zinc (Zn) ions. The quality of the synthesized crystals is characterized by the high purity of the final product in both the sonochemical and control (without sonication) methods, as the FT-IR spectra do not show any additional peaks or impurities. This finding is in good agreement with the results of the analysis. The elemental (CHN) is consistent, confirming an almost identical chemical composition for products synthesized under different conditions (19, 20).

3.2 .Absorption test of Sunset Yellow and Carmoisine dyes with nano-sorbent

Absorption experiments were conducted on a laboratory scale and a jartest device was used to mix the mock and absorbent solutions. In these experiments, the effects of various factors including pH, contact time, amount of absorbent and initial concentration of the tested dyes, competitive adsorption of Sunset Yellow and Carmoisine, and isotherm models on the absorption of Sunset Yellow and Carmoisine dyes were investigated. In order to determine the most appropriate wavelength to measure the concentrations of the studied dyes, the standard method was used. Finally, the most appropriate wavelength that gave maximum absorption for Sunset Yellow was determined to be 458 nm. To prepare synthetic wastewater, first a 1000 ppm solution of Sunset Yellow and Carmoisine dyes was made as a standard solution, which was placed on a stirrer for 3 minutes at 180 rpm to homogenize, and then this

solution was used as a stock solution to prepare samples with concentrations of (5, 10, 20, 30, 40, and 50 mg/L), which are the same as the initial concentrations or C0.

3.3. Effect of pH and adsorbent amount on the removal process

Figure 6 shows that to achieve higher efficiency in removing Sunset Yellow from the solution, the pH of the solution should be around 7 and the amount of nanocomposite should be 0.25 g. Under these conditions, a higher removal percentage is obtained. Conversely, as the pH increases and the amount of nanocomposite decreases, the removal percentage decreases. The first graph (A) is a three-dimensional graph showing the combined effect of pH and adsorbent amount on the removal percentage of Sunset Yellow. The highest removal efficiency is obtained at pH 7 and a nanocomposite amount of 0.25 g. As the pH increases or the number of adsorbent decreases, the removal efficiency decreases. The second graph (B) is a contour plot showing the same relationship in two dimensions. The red areas indicate higher removal percentages, while the blue areas indicate lower efficiencies. Again, the optimal conditions are at pH 7 and a nanocomposite amount of 0.25 g.

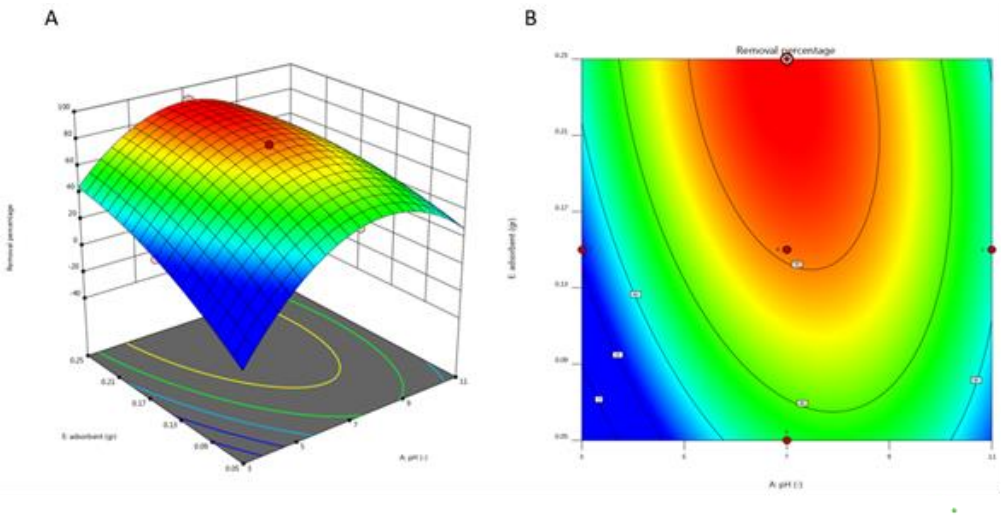

Fig. 7. Effect of pH and adsorbent amount on the removal efficiency of Sunset Yellow dye. The 3D plot (A) and contour plot (B) show that the highest removal efficiency is obtained at pH 7 and with 0.25 g of nanocomposite. The removal efficiency decreases with increasing pH or decreasing adsorbent amount.

3.4 Combined diagram of the effect of pH and mixing speed on the removal process

Figure 7 shows that to achieve higher efficiency in removing Sunset Yellow from the solution, the pH of the solution should be in the range of 7 and the mixing speed of the solution should be around 600 rpm. Under these conditions, the removal percentage reaches its maximum. However, the results of the experiments show that the mixing speed did not have a significant effect on the removal efficiency and its changes did not significantly affect the results. This figure shows the optimal conditions for achieving the highest removal efficiency of Sunset Yellow from the solution. According to the graphs:

• pH: The highest removal efficiency is obtained at pH 7, where the removal percentage reaches its peak.

• Mixing speed: Increasing the mixing speed to 600 rpm does not have a significant effect on the removal efficiency, as can be seen from the smoothness of the graph surface and the lack of significant changes in the contour plot. These findings indicate that adjusting the pH to around 7 is essential to maximize the removal efficiency of Sunset Yellow, while changing the mixing speed within the tested range does not have much effect on the removal process.

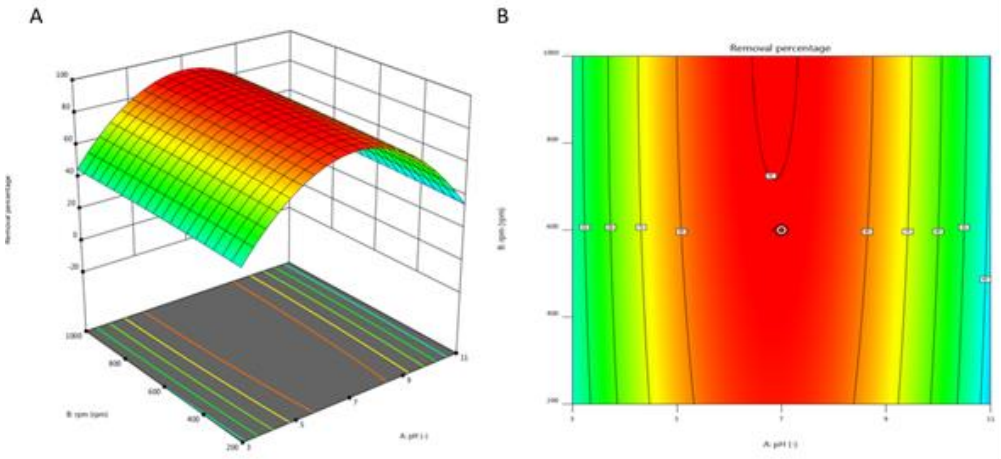

Fig. 8.A) 3D plot showing the interaction of pH and mixing speed (rpm) on the percentage removal of Sunset Yellow dye from solution. The plot shows that the highest removal efficiency is achieved when the pH is around 7 and the mixing speed is around 600 rpm. B) Contour plot corresponding to the 3D plot in panel A shows the percentage removal.

3.5. Combined diagram of the effect of pH and time on the removal process

The combined effect of pH and time on the removal process is shown in Figure 10. According to the results obtained from the experiments, the optimal conditions for achieving the highest removal efficiency are pH 7 and a reaction time of 90 minutes. Under these conditions, the highest removal percentage is observed. With decreasing time, the removal percentage decreases and also with increasing time beyond the optimal limit of 90 minutes, the removal efficiency decreases again. The figure presented shows the combined effect of pH and reaction time on the removal percentage of Sunset Yellow dye. The three-dimensional diagram shows that the highest removal percentage is obtained when the pH of the solution is 7 and the reaction time is 90 minutes. The less the reaction time is, the lower the removal percentage decreases. Also, if the reaction time exceeds 90 minutes, the removal efficiency decreases again. The contour diagram shows the same relationship in two dimensions and identifies the areas with the optimal removal efficiency using contour lines. It can be clearly seen that the optimal conditions are around pH 7 and time 90 minutes

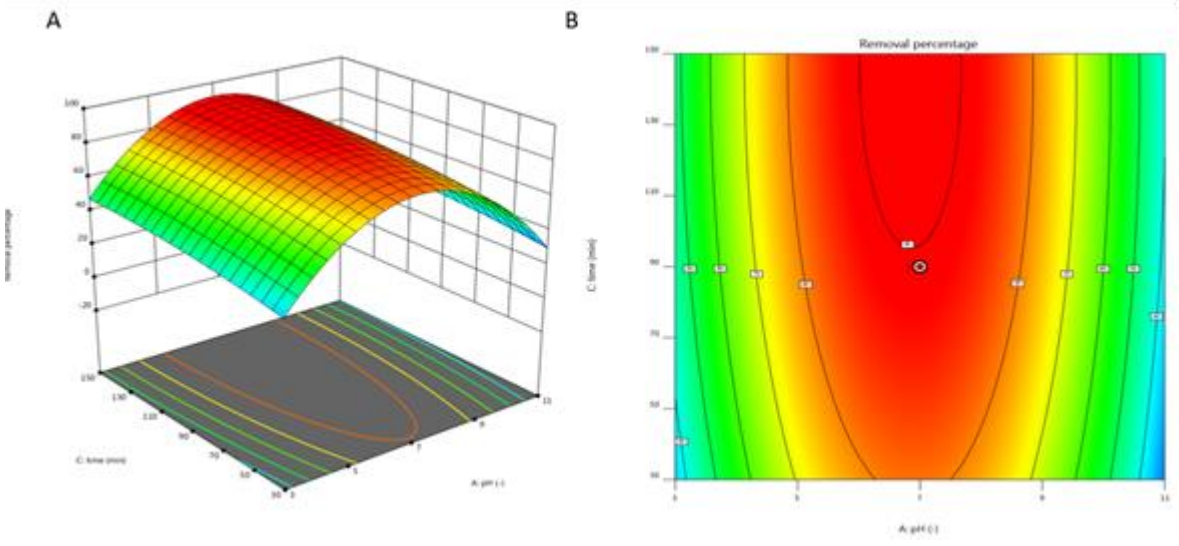

Fig. 9. (A) Three-dimensional response surface plot showing the combined effect of pH and time on the percentage removal of Sunset Yellow dye. The highest removal efficiency is obtained at pH 7 and a reaction time of 90 min. (B) Two-dimensional contour plot showing the same effects and indicating the areas of optimal removal efficiency with contour lines.

3.6.Combined diagram of the effect of the amount of adsorbent and the amount of Sunset Yellow dye on the removal process

As shown in Figure 9, to achieve the highest removal efficiency of Sunset Yellow from the solution, it is necessary to increase the amount of nanocomposite and reduce the concentration of the pollutant in the environment. The best result was obtained in the presence of 0.25 g of nanocomposite and a concentration of 40 mg/L of pollutant. The three-dimensional diagram shows the effect of the amount of adsorbent (nanocomposite) and the concentration of pollutant (Sunset Yellow) on the removal percentage. The highest removal efficiency is observed at the condition of 0.25 g of nanocomposite and a concentration of 40 mg/L of pollutant. The contour plot shows a two-dimensional view of the same parameters, in which the areas with high removal efficiency are shown in red. The optimal conditions for maximum removal are in the presence of 0.25 g of nanocomposite and a concentration of 40 mg/L of pollutant.

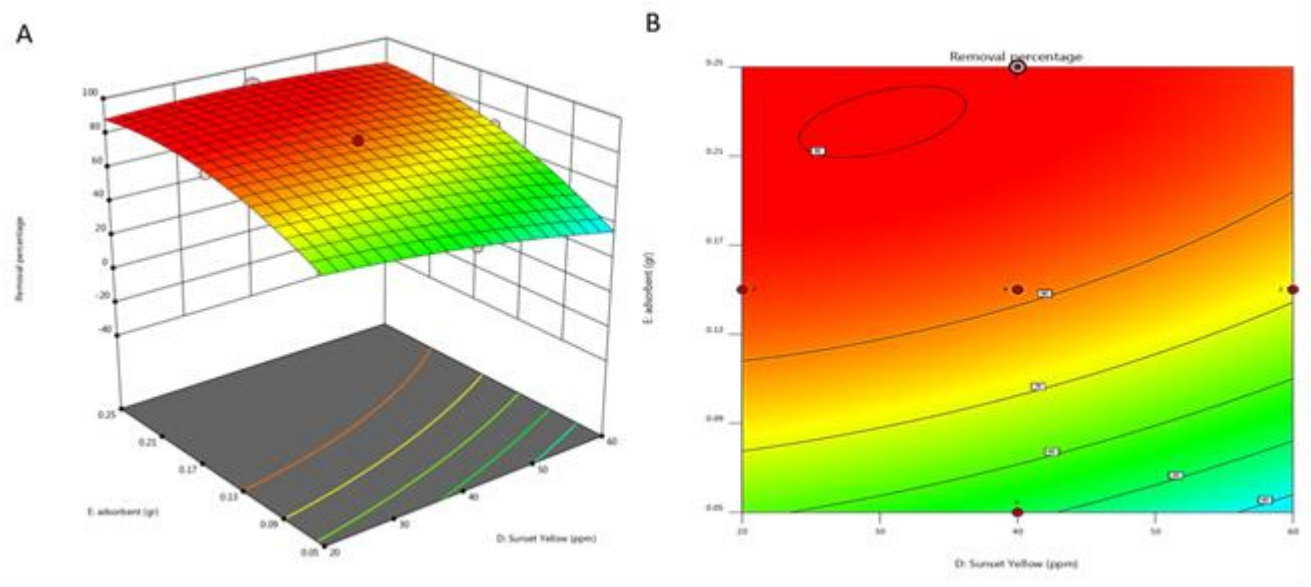

Fig. 10. A) 3D response surface plot showing the effect of nanocomposite adsorbent amount and Sunset Yellow pollutant concentration on removal efficiency. B) Contour plot of the same parameters showing the optimal conditions for maximum removal efficiency at 0.25 g nanocomposite and 40 mg/L pollutant concentration.

3.7. Reusability

To investigate the reusability of Sunset Yellow, the nano-framework precipitate was collected during the regeneration stage and reused for dye removal during the sorbent optimization experiments. The results of the nano-sorbent reuse are summarized in Table 3.

Table 3. Reusability of nano-sorbent for absorbing Sunset Yellow

Cycle	C_0 (mg/L)	C_eq (mg/L)	Removal %	Time (min)
1st	1.8	0.004	99.7	120
2nd	0.6	0.02	96.6	120
3rd	0.02	0.006	70	120
4th	0.02	0.008	60	120

According to the results of four consecutive cycles of adsorption/desorption of Sunset Yellow by methanol, the removal efficiency of Sunset Yellow decreased after four stages of adsorption and desorption. The amount of Sunset Yellow absorbed by the nano-sorbent decreased from 90.4% in the first cycle to 46.1% in the fourth cycle. The amount of Sunset Yellow absorbed by the nano-sorbent decreased from 95.6% in the first cycle to 37.5% in the fourth cycle.

Competitive effect of simultaneous absorption of sunset yellow and crimson dyes

To determine the competitive effect of simultaneous dye adsorption, two samples were prepared with the optimal characteristics of each dye obtained in the previous steps. It is worth noting that in each sample there was an optimal concentration of both dyes. Then, each sample was carried out according to the optimal conditions of each dye and the amount of residual Sunset Yellow and Carmosin dyes was measured for each sample. From the results, it was observed that the highest percentage of Sunset Yellow dyes was removed using the nano-sorbent at pH = 5 and this efficiency decreased at higher and lower pH values. Therefore, the optimal pH for the removal process in this study is pH = 5. From the results, it was observed that the highest percentage of Sunset Yellow dye removal occurred with a concentration of 0.5 g/L of the nano-sorbent. The results showed that the highest percentage of removal for Sunset Yellow dye was done by the nano-sorbent in 40 minutes.

3.8. Adsorption isotherm for Sunset Yellow dye using Zn-MOF frameworks

Table 4 shows comprehensive data from the adsorption isotherm experiment, which includes various initial concentrations from 20 to 60 mg/L. Analysis of these data provides important information about the adsorption mechanism and the performance of the adsorbent.

Table 4. Effect of initial concentrations on the percentage of removal of Sunset Yellow food coloring from aqueous media by nano-adsorbent for isotherm studies

C_o(mg L^{-1})	C_e(mg L^{-1})	Removal percentage	q_e(mg g^{-1})	1/ce	1/qe	C_e/q_e
20	3.13	84.35	1.687	0.319	0.592	1.855
30	6.18	79.40	2.382	0.161	0.419	2.594
40	10.70	73.25	2.930	0.093	0.341	3.651
50	17.15	65.70	3.285	0.058	0.304	5.220
60	22.97	42.57	3.703	0.043	0.270	6.203
Ln C_e	Ln q_e	Ɛ (J/ mole)	$Ɛ^2$	logqe	log ce	Ce / C_0
1.141	0.522	685.97	470560	0.22711	0.4955	0.156
1.821	0.867	369.85	136793	0.37694	0.7909	0.206
2.370	1.075	220.32	48541	0.4668	1.0293	0.267
2.841	1.189	139.68	19512	0.51653	1.2342	0.343
3.134	1.309	104.30	10880	0.56855	1.3611	0.382

The results presented in this table show that as the initial concentration increased from 20 to 60 mg/L, the adsorption capacity (qe) increased from 1.687 to 3.703 mg/g. This trend indicates the positive relationship between initial concentration and adsorption capacity, which is commonly observed in adsorption processes.

Based on the results obtained:

• Langmuir shows the best fit and shows that the adsorption of Sunset Yellow is a monolayer adsorption pattern on a uniform surface.

• Freundlich and Temkin also show good fit, with the Freundlich model representing the adsorption of heterogeneous surfaces and the Temkin model representing molecular

interactions. • DKR shows that the adsorption is mainly physical and the model fits the data well. These results show that the adsorption of Sunset Yellow is best fit with the Langmuir and Freundlich models.

References

[1]. Schwarzenbach, R. P., Escher, B. I., Fenner, K., Hofstetter, T. B., Johnson, C. A., Von Gunten, U., & Wehrli, B. The challenge of micropollutants in aquatic systems. *Science,* 313(5790) (2006) 1072-1077.

[2]. Yaseen, D. A., & Scholz, M. Textile dye wastewater characteristics and constituents of synthetic effluents: a critical review. *International Journal of Environmental Science and Technology,* 16(2) (2019) 1193-1226.

[3]. Brillas, E., & Martínez-Huitle, C. A. Decontamination of wastewaters containing synthetic organic dyes by electrochemical methods. An updated review. *Applied Catalysis B: Environmental,* 166(2015) 603-643.

[4]. Holkar, C. R., Jadhav, A. J., Pinjari, D. V., Mahamuni, N. M., & Pandit, A. B. A critical review on textile wastewater treatments: Possible approaches. *Journal of Environmental Management,* 182(2016) 351-366.

[5]. Crini, G. Non-conventional low-cost adsorbents for dye removal: A review. *Bioresource Technology,* 97(9) (2006) 1061-1085.

[6]. Ali, I. New generation adsorbents for water treatment. *Chemical Reviews,* 112(10) (2012)5073-5091.

[7]. Gupta, V. K., & Saleh, T. A. Sorption of pollutants by porous carbon, carbon nanotubes and fullerene- an overview. *Environmental Science and Pollution Research, 20*(5) (2013)2828-2843.

[8]. Kyzas, G. Z., & Matis, K. A. Nanoadsorbents for pollutants removal: A review. *Journal of Molecular Liquids,* 203 (2015)159-168.

[9]. Wang, J., Chen, B., & Xing, B. Wrinkle-or-ripple-based selective adsorption of naphthalene on single-layer graphene. *Environmental Science & Technology,* 50(6) (2016) 3311-3318.

[10]. Qutub, N., Singh, P., Sabir, S., Sagadevan, S., & Oh, W. C. Enhanced photocatalytic degradation of organic dyes by metal–organic frameworks (MOFs) and their composites: A review. *Journal of Environmental Chemical Engineering*, 10(3) (2022) 107508.

[11]. Nizamuddin, S., Siddiqui, M. T. H., Mubarak, N. M., Baloch, H. A., Abdullah, E. C., & Mazari, S. A. Advanced nanomaterials for dye removal. *In Advances in Nano-Fertilizers and Nano-Pesticides in Agriculture* .(2021) 471-494. Woodhead Publishing.

[12]. Chung, K. T. Azo dyes and human health: A review. *Journal of Environmental Science and Health, Part C,* 34(4) (2016) 233-261.

[13]. Forgacs, E., Cserháti, T., & Oros, G. Removal of synthetic dyes from wastewaters: a review. *Environment International*, 30(7) (2004) 953-971.

[14]. Robinson, T., McMullan, G., Marchant, R., & Nigam, P. Remediation of dyes in textile effluent: a critical review on current treatment technologies with a proposed alternative. *Bioresource Technology*, 77(3) (2001)247-255.

[15]. Yagub, M. T., Sen, T. K., Afroze, S., & Ang, H. M. Dye and its removal from aqueous solution by adsorption: A review. *Advances in Colloid and Interface Science, 209*(2014) 172-184.

[16]. Gupta, V. K., Pathania, D., Agarwal, S., & Singh, P. Adsorptive remediation of Cu (II) and Ni (II) by microwave assisted H3PO4 activated carbon. *Arabian Journal of Chemistry,* 10 (2013) S2966-S2975.

[17]. Mishra, S., & Maiti, A. The efficacy of bacterial species to decolourise reactive azo, anthroquinone and triphenylmethane dyes from wastewater: a review. *Environmental Science and Pollution Research,* 25(9) (2018) 8286-8314.

[18]. De Gisi, S., Lofrano, G., Grassi, M., & Notarnicola, M. Characteristics and adsorption capacities of low-cost sorbents for wastewater treatment: A review. *Sustainable Materials and Technologies,* 9(2016) 10-40.

[19]. Khan, I., Saeed, K., & Khan, I. Nanoparticles: Properties, applications and toxicities. *Arabian Journal of Chemistry,* 12(7) (2019)908-931.

[20]. Hasanzadeh, M., Simchi, A., & Shahriyari Far, H. Nanoporous composites of metal-organic frameworks for advanced water treatment applications. *Separation and Purification Technology,* 237(2020) 116355.

[21]. Yaghi, O. M., O'Keeffe, M., Ockwig, N. W., Chae, H. K., Eddaoudi, M., & Kim, J. Reticular synthesis and the design of new materials. *Nature,* 423(6941) (2003) 705-714.

[22]. Furukawa, H., Cordova, K. E., O'Keeffe, M., & Yaghi, O. M. The chemistry and applications of metal-organic frameworks. *Science,* 341(6149) (2013) 1230444.

[23]. Haque, E., Jun, J. W., & Jhung, S. H. Adsorptive removal of methyl orange and methylene blue from aqueous solution with a metal-organic framework material, iron terephthalate (MOF-235). *Journal of Hazardous Materials,* 185(1) (2011) 507-511.

[24]. Katz, M. J., Brown, Z. J., Colón, Y. J., Siu, P. W., Scheidt, K. A., Snurr, R. Q., ... & Hupp, J. T. A facile synthesis of UiO-66, UiO-67 and their derivatives. *Chemical Communications,* 49(82) (2013) 9449-9451.

[25]. Wang, C., Liu, X., Keser Demir, N., Chen, J. P., & Li, K. Applications of water stable metal-organic frameworks. *Chemical Society Reviews,* 45(16) (2012) 5107-5134.

[26]. Li, J., Wang, H., Yuan, X., Zhang, J., & Chew, J. W. Metal-organic framework membranes for wastewater treatment and water regeneration. *Coordination Chemistry Reviews,* 404 (2019) 213116.